Crack Path in Particulate Reinforced Metal Matrix Composites

Fernand Ellyin

Advanced Composite Materials Engineering Group

Department of Mechanical Engineering, University of Alberta

Edmonton, AB, Canada, T6G 2G8

Fernand.ellyin@ualberta.ca

ABSTRACT. Inhomogeneous distribution of particles is unavoidable in the micro-structural scale of particulate reinforced metal matrix composites (PMMCs). This has a considerable influence on the short crack, and near threshold long crack growth. Generally particle clusters and often large particles are sites of short crack initiation. Once a short crack is initiated, its growth is highly influenced by the heterogeneous distribution of particles. Two characteristics distinguish the short crack behavior in PMMCs. First, both the direction and growth rate are highly affected by particles, especially the large ones. Second, the size of short cracks which exhibit micro-structure-sensitivity is much longer than that of the matrix material. In the case of long cracks the growth rate in the intermediate K_{max} (or ΔK) is independent of particles. However, particles increase resistance to crack growth at the low (near threshold) values. Based on the observed behavior of short and long cracks in PMMCs, six crack growth regimes have been identified. Each phase boundary corresponds or is related to an overall material property.

INTRODUCTION

Particle-reinforced metal matrix composites (PMMCs) are good candidate materials where high strength to weight ratio is required. Hence, they have found applications in the aerospace and ground transportation industries as well as recreational/sports equipments. Generally PMMCs are produced by adding ceramic particles such as alumina (Al_2O_3) or silicon carbide (SiC) into molten metals (e.g. aluminum alloys or titanium alloys) and mixed to disperse particles as uniformly as possible. Powder

metallurgy processing methods have also been used in the production of PMMCs. The resulting PMMCs have, in general, isotropic properties in the *macroscopic* scale. Compared with their fiber-reinforced counter parts, the production cost of PMMCs is much lower, and most of the present manufacturing techniques of metals and alloys can be easily adapted to PMMCs.

By adding particles in sufficient volume fraction (e.g. > 10%) one notes a substantial increase in stiffness and yield strength and to a lesser extent ultimate strength in comparison to the unreinforced alloy. However, the ductility of the PMMCs is generally reduced when compared with the matrix material. The reduction in ductility increases with the increase of the particle volume fraction, see Lloyd [1]. Thus, there is a compromise between the stiffness increase and ductility reduction, and for this reason the particle volume fraction is generally kept below 30%. The reduction in ductility arises from the non-uniform size and distribution of particles in the microscopic scale, which results in localized damage sites, e.g. see Davidson [2]. Furthermore, due to the mismatch of thermal and mechanical properties of the matrix metals and reinforcing ceramic particles, internal residual stresses are generated during the processing of PMMCs. Through proper post-processing heat treatment, one attempts to reduce the internal residual stress without compromising the increase in yield strength and stiffness.

The deformation of PMMCs under monotonic and cyclic loading is described in the section which follows. In addition to the experimental results, predictions by a micro-mechanical approach are also presented. Following this, the resistance of PMMCs to short and long crack growth will be elucidated. It will be shown that direction and growth rate of short cracks is greatly influenced by the large particles. In contrast, particles are ineffective in impeding the growth of a long crack. The results presented here are a compilation of an extensive investigation on the mechanical properties of PMMCs carried out in our laboratory, with focus being on the growth of cracks. Readers interested in other aspects, e.g. fatigue resistance and damage mechanisms or the influence of multiaxial loading are encouraged to consult a recent book chapter [3] and references cited therein.

UNIAXIAL STRESS-STRAIN RELATIONS

PMMCs generally show an elastoplastic deformation behavior since one of the constituents (metal matrix) is an elastoplastic material while the other (ceramic particles) has a linear stress-strain relation for most of its range. However, dispersion of ceramic particles in metallic matrices can cause micro structural changes such as higher dislocation density, Christman [4], smaller average grain size, Poza [5], etc. Consequently, the PMMCs can have a more complex deformation behavior, which may not be observed in pure metals or alloys.

Figure 1 shows a typical micrograph of 6061Al/22% vol. Al_2O_3 composite. The average particle size is 16 μm. One notes inhomogeneous distribution of particles in the *micro-scale* with fractured large particles. As well there are matrix rich regions.
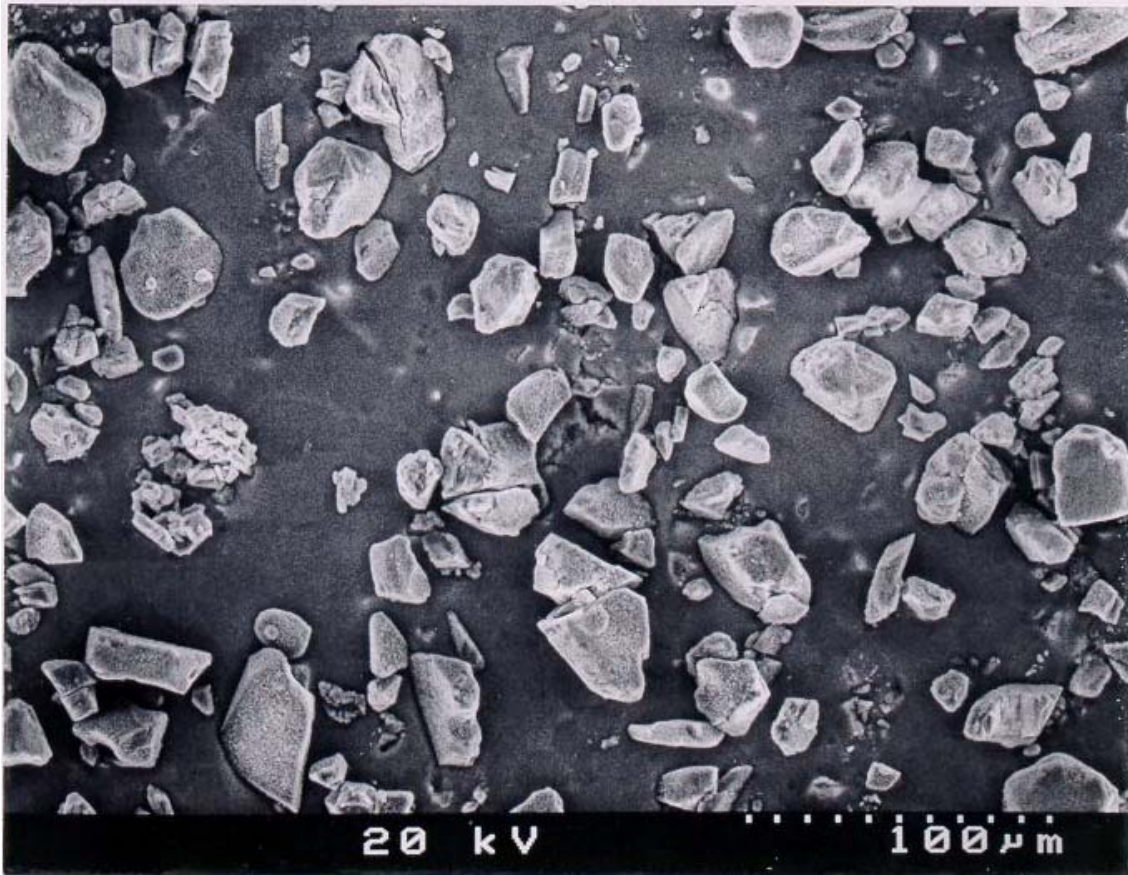
Figure 1. A typical micrograph of 6061Al/22% vol. Al_2O_3 composite

There have been numerous papers published on the mechanical and fatigue behavior of PMMCs, for example, sees references [3, 6, 7] where further sources are cited. In the following some typical experimental results of an alumina particle reinforced 6061aluminum alloy with different heat-treatment conditions will be presented (Xia et al. [6], Meijer et al. [7]).

Monotonic uniaxial stress-strain curves of PMMC, 20% Al_2O_3 6061-T0 (annealed) and 20% Al_2O_3 6061-T6 (solution heat-treated and precipitation hardened) and the corresponding unrienforced aluminum alloys with the same heat-treatment conditions, are shown in Fig. 2. It is seen that adding the ceramic particles increases the stiffness and strength (elastic modulus, 0.2% offset yield stress, and ultimate strength). It is also

noted that the proportional limit of the composite becomes lower than that of the matrix alloy. For the 6061-T0 alloy it is 34 MPa, while for that of the 20% Al_2O_3 6061-T0 PMMC is 20 MPa. For the T6 treatment, the values are 264 MPa and 185 MPa, respectively. Therefore, the stress-strain curves for the composites have a larger elastic-plastic transition region which results in greater strength, see Fig. 2. This implies that plastic deformation occurs in the matrix of the composite at a lower global stress level than that of the matrix alloy. This can be attributed to the local stress concentrations due to existence of the particles.
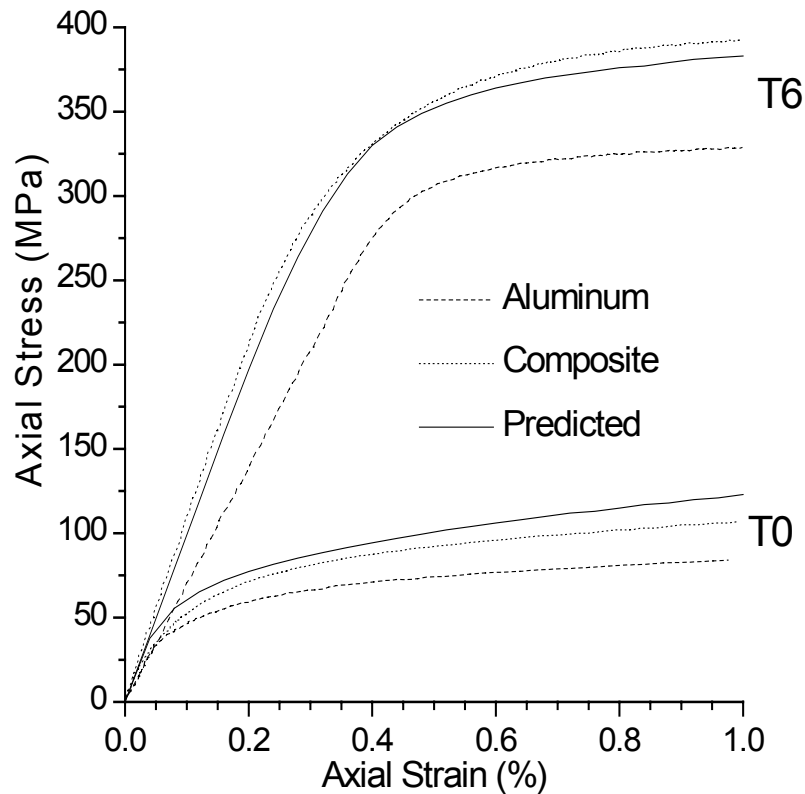
Figure 2. Experimental and predicted monotonic stress- strain curves of the matrix alloy, 6061 Al and 20% Al_2O_3 6061 Al composite for two heat treatment conditions, from ref. [7].

The experimental results depicted in Fig. 2 were compared with those found using a three dimensional finite element analysis on a representative unit cell. A special material model, capable of accurately describing the behavior of metals under complex multiaxial loadings was used to simulate the elastic-plastic aluminum matrix, Ellyin [8]. It is seen in Fig. 2 that the unit cell model provides an accurate prediction of the composite behavior.

Figure 3 shows the first ten cycles of fully-reversed, strain-controlled stress/strain loops of the above two heat-treated PMMCs. The relative change of stress range with the increasing number of cycles indicates the degree of cyclic strain hardening. In the case of the specimen with T6 heat treatment ($\Delta\varepsilon / 2 = 0.4\%$) cyclic hardening was observed only in the first two cycles. The stress range remained stable (with a small amount of softening) until the failure (N_f =1214 cycles). For the T0 specimen ($\Delta\varepsilon / 2 = 0.3\%$) the stress range increased steadily in the first 10 cycles and thereafter it was relatively stable up to about 100 cycles. Following this, the cyclic-hardening process resumed again and lasted until failure of the specimen (N_f =1430 cycles). All these observations are very similar to that of the unreinforced matrix material. There is a large amount of cyclic hardening for the under-aged or annealed matrix materials while very little for the fully-aged ones.
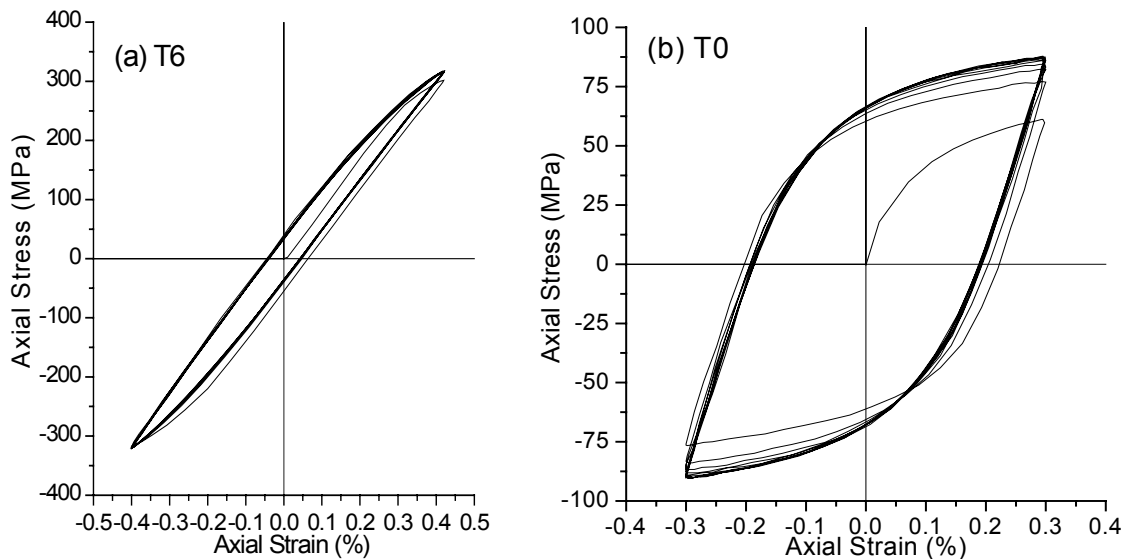
Figure 3. Uniaxial cyclic stress-strain loops of 20% Al$_2$O$_3$ 6061 Al PMMC

(a) T6 heat-treatment (b) T0 heat-treatment, from [6].

SHORT CRACK GROWTH

In general particle clusters containing large particles are sites of short crack initiation see Fig. 1. Once a short crack is initiated, either by residual stresses during manufacturing process or by external loads, its growth is highly influenced by the heterogeneous distribution of particles. Two characteristics distinguish the short crack

behavior in PMMCs. First, both the direction and growth rate are highly affected by particles, especially the large ones. Second, the size of short cracks which exhibits micro-structure-sensitivity is much longer than that in metals and alloys. For example, Fig. 4 shows the growth of an initially short crack of $a_i \approx 120\,\mu m$ under a maximum stress of $\sigma_{max} = 110\,MPa$, $\Delta\sigma = 150\,MPa$ and $R = -0.35$, Li and Ellyin [9]. It is seen that the crack growth up to three times its initial length is highly influenced by the particles as shown in the upper part of the figure. The fracture of an average sized particle in the crack path (from D to E) plays a key role in maintaining the crack growth.
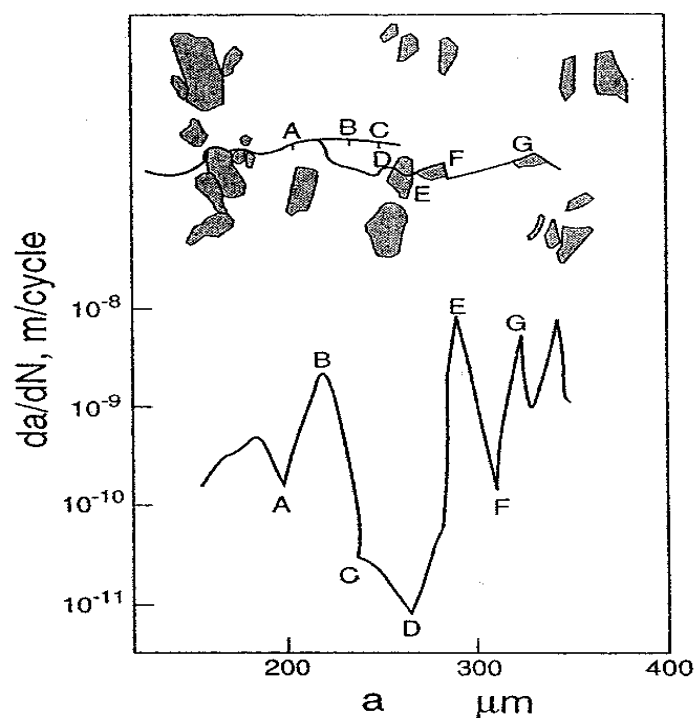
Figure 4. Short crack path and its growth rate vs. crack length, from [9].

The effect of a nearby particle on the stress/strain distribution in front of an advancing crack was investigated by a finite element analysis in Li and Ellyin [10]. In this analysis the particle distribution in the PMMC was approximated by a periodic array consisting of body-centered cubic lattice with spherical particles. The size of each particle was taken to be equal to the average particle size of the composite. The distance among particles was determined from the volume fraction of the particle which were equal or greater than the average size [10]. Figure 5 shows the effect of a nearby particle on the stress distribution of an approaching short crack. Crack tip stress contours in the

PMMC are plotted and compared with those in the matrix alloy under the same loading condition and crack geometry. It is observed that the presence of a particle in the crack path causes the maximum stress to shift from the crack tip to the particle. That is, the crack tip stress decreases and the normal tensile stress at the particle increases, especially on the part facing the crack tip. Furthermore, there is an increase in the stress magnitude in the space between the two particles ahead of the short crack, Fig. 5.
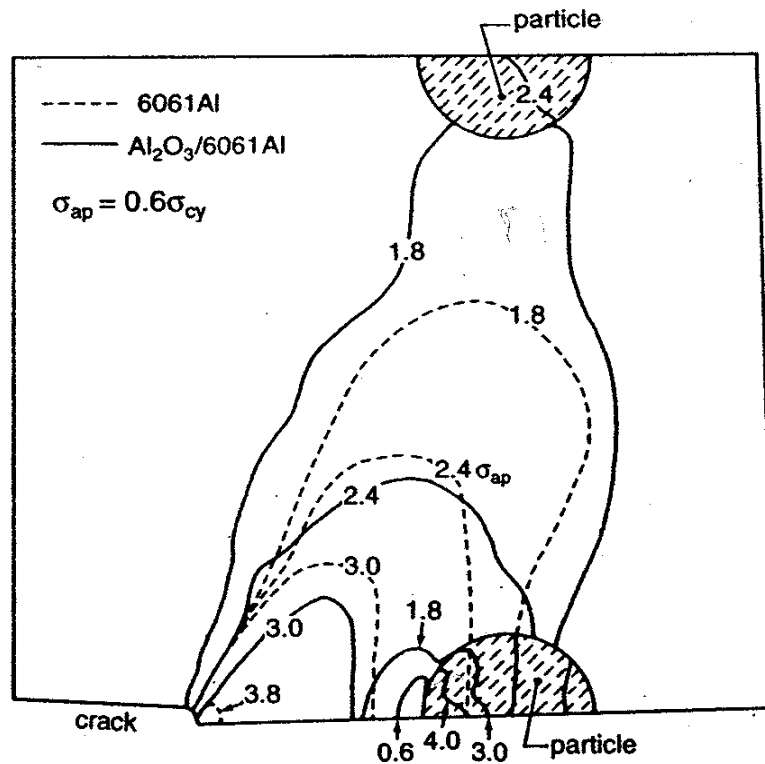
Figure 5. Stress contours ahead of a short crack in $Al_1O_3/6061$ Al and in pure 6061 Al alloy of the same crack length and under same applied stress, from [10].

The plastic zone size ahead of a crack is also affected by the presence of the particles. The plastic zone size decreases, as a crack approaches a particle on its path. Since the crack growth results from the damage caused by irreversible movement of dislocations in the cyclic plastic zone, the change in the crack tip plastic zone size and shape will promote a change in the crack growth as the crack approaches a particle, Li and Ellyin [10].

An example of a short crack growth and its arrest is shown in Fig. 6. Here an initial crack of length $a_i = 180\,\mu m$ is subjected to a maximum stress of $\sigma_{max} = 99\,MPa$ (approximately equal to the fatigue limit of the material). The crack growth pattern

follows the drastically varying rate usually observed in the short crack growth (cf. Fig. 4). In this case, however, after growing for about $100\,\mu m$, the crack tip reaches a large particle and ceases to propagate. The local stress state is not high enough to fracture the particle.

It has been shown that short cracks up to 400 microns in length propagate in shear dominated mode at a maximum stress level below the fatigue limit of the composite material until they are permanently trapped by the surrounding particles. The microstructure sensitivity of short crack growth in PMMCs decreases as the short crack length and/or the applied stress range increase.
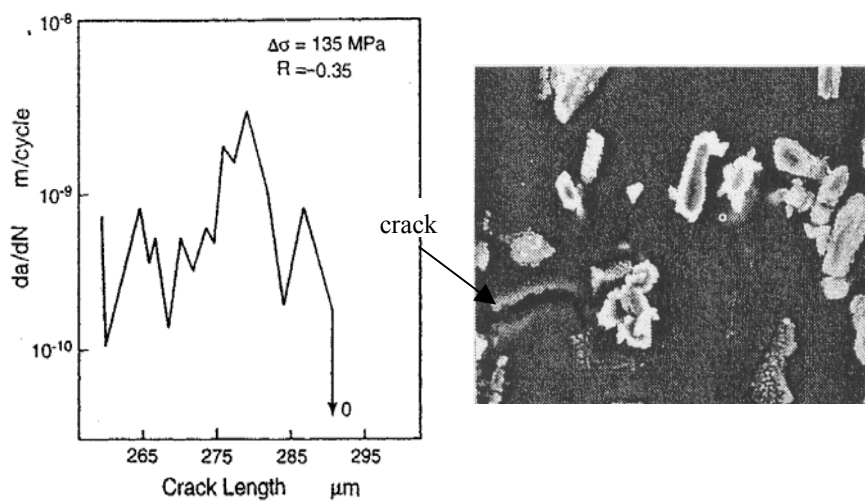
Figure 6. A short crack growth and its arrest by a cluster of particles under $\sigma_{max} = 99$ MPa, R = -0.35, from [10].

From the foregoing discussion we can distinguish two regimes of short crack growth, one which has sufficiently high crack tip stress field to drive it past the particle, and the second which is blocked by the particle(s). The latter was termed pre-cease short crack growth in [10].

LONG CRACK GROWTH

The crack growth rate, da/dN, versus the maximum stress intensity factor, K_{max}, for cracks longer than 3 mm is shown in Fig. 7, in a log-log scale, for composites with 10% and 20% particle volume fraction and for the pure matrix alloy, respectively. It is seen

that in the intermediate stress intensity, $K_{max} > 8$ MPa(m)$^{1/2}$, all the data fall on a straight line with a narrow scatter band. This indicates that the growth rate in the intermediate K_{max} (or ΔK) is independent of particles. However, in the near threshold region, there are three distinct growth curves for each material. The threshold stress intensity factor varies from 4.5 MPa(m)$^{1/2}$ for the matrix to 6.5 MPa(m)$^{1/2}$ for the 10% volume fraction composite to 7.5 MPa(m)$^{1/2}$ for that of 20%. Thus, the threshold stress intensity increases by about 44% for the first 10% particulate reinforcement and by about 22% for the next 10% reinforcement compared to the matrix threshold value.
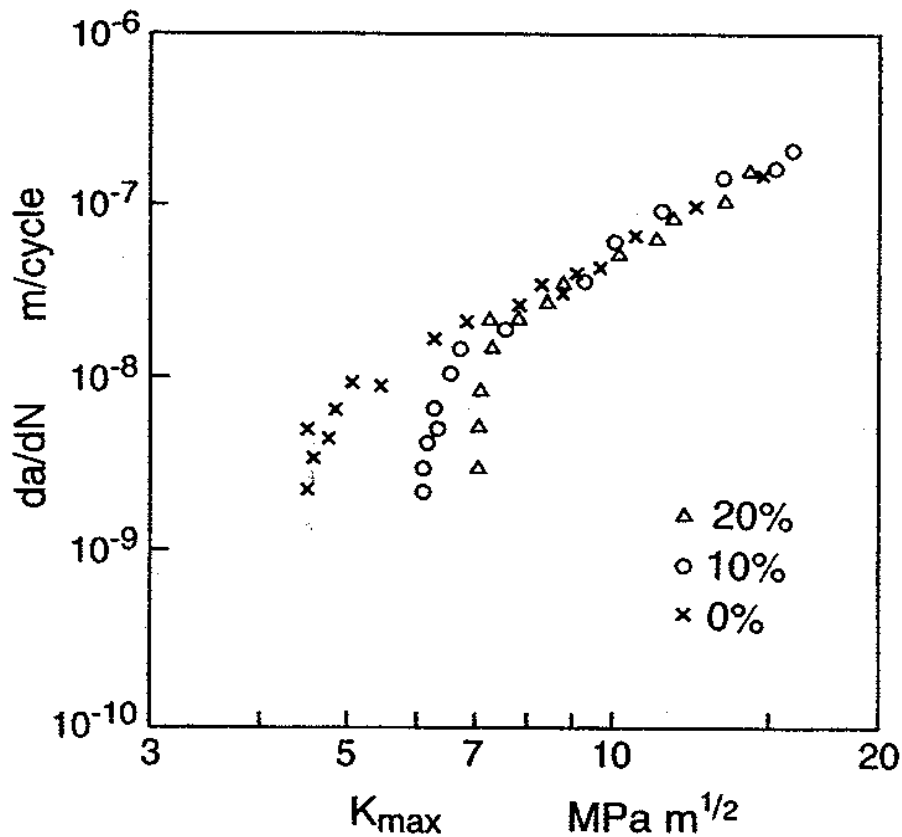
Figure 7. Variation of the crack growth rate with the maximum stress intensity, K_{max}, at load ratio of R = −0.4, for the Al$_2$O$_3$/6061-T6 Al composites and for the 6061-T6 aluminum alloy, from [11].

This is a fairly substantial increase in the threshold stress intensity which indicates an increased resistance to crack growth at the low (near threshold) values due to the presence of particles.

This type of behavior has also been reported for silicon carbide particle-reinforced aluminum, e.g. see Shang and Ritchie [12]. The reason for the ineffectiveness of particles to resist crack growth in the intermediate stress intensity factor will be described as follows.

DETERMINATION OF CRACK GROWTH RATE

Matrix Material

For an elastic-plastic material with a power law strain hardening, a crack growth model was derived involving mechanical, cyclic, fatigue properties as well as a length parameter associated with the microstructure, see Ellyin [7]. The crack propagation model has the form of,

$$\frac{da}{dN} = 2\delta * \left[\frac{\Delta K^2 - \Delta K_{th}^2}{4\psi E \sigma_f' \varepsilon_f' \delta *} \right]^{1/\beta} \tag{1}$$

where σ_f' and ε_f' are the fatigue strength and ductility coefficients and $\beta = -(b+c)$ with b and c appearing as the exponents in the Coffin-Manson fatigue life relationship, $\delta *$ is a microstructural length parameter indicating the extent of "process zone" and is generally of the order of the material's grain size, and $\psi = \psi(n')$ is a parameter, function of cyclic strain hardening exponent, n', and depends on the chosen crack tip fields, Ellyin [13]. The crack growth model, Eq. (1) was obtained based on a material's capacity to absorb a certain amount of plastic strain energy. In the intermediate ΔK range, where ΔK_{th}^2 can be neglected compared to ΔK^2, then (1) reduces to,

$$\frac{da}{dN} = 2\delta * \left[\frac{\Delta K}{(4\psi E \sigma_f' \varepsilon_f' \delta *)^{1/2}} \right]^{2/\beta} \tag{2}$$

A number of empirically proposed crack growth models can be derived as a particular case of relation (2). It is interesting to note that for the aluminum alloy $2/\beta \approx$ 3.2 and the slope of the straight line in Fig. 7, is 3.3.

Fine and Davidson [14] have proposed an energy-based crack growth law,

$$\frac{da}{dN} = \frac{A\,\Delta K^{4}}{G\,\sigma_{y}\,2U} \tag{3}$$

where A is a constant, G is the shear modulus and U is an effective surface energy. For the matrix material, the constants in (3) can be determined by equating the right-hand side of Eqs. (2) and (3), see reference [8]. The exponent 4 in Eq. (3) over estimates the slope of the linear portion, therefore, we can write (3) in the form of,

$$\left[\frac{da}{dN}\right]_{m} = \frac{A(\Delta K)^{2/\beta}}{G_{m}\sigma_{ym}\,2U_{m}} \tag{4}$$

In the above the subscript m is used to indicate the matrix material.

Composite Material

For a particle-reinforced composite, U in Eq. (3) could be expressed as,

$$U_{c} = U_{m}(1 - f_{a}) + U_{p}f_{a} \tag{5}$$

where subscripts c, m and p refer to the composite, matrix and particle, respectively, and f_{a} is the area fraction of particles. Based on a uniform particle distribution,

$$f_{a} = f_{v}^{2/3} \tag{6}$$

The monotonic yield stress of the PMMC, σ_{yc}, varies with the particle volume fraction according to the following empirical formula,

$$\sigma_{yc} = \sigma_{ym}(1 + f_{v}^{\alpha})/C \tag{7}$$

where α and C are constants equal to 2.1 and 1.14, respectively for the Al_2O_3/6061 A1, and σ_{ym} is the yield stress of 6061 A1 matrix [11].

Substituting from (6), (7) and (5) into (3) with the modified exponent, and noting that $U_p << U_m$, the crack growth rate of the composite is given by

$$\left[\frac{da}{dN}\right]_c = \frac{A(\Delta K)^{2/\beta}}{G_c \sigma_{ym} 2 U_m [(1+f_v^a)(1-f_v^{2/3})/C]} \tag{8}$$

In the above the subscript c denotes the composite material.

A comparison of the crack growth rate of the composite with that of the same length crack in the matrix alloy under the same ΔK, is obtained by dividing (8) by (4), which gives

$$\frac{(da/dN)_c}{(da/dN)_m} = \frac{1.14\, G_m}{G_c[(1+f_v^\alpha)(1-f_v^{2/3})]} \tag{9}$$

The right-hand-side of (9) is approximately equal to 1, and thus, the growth rate of the composite approaches that of the matrix alloy as seen in Fig. 7.

Crack –phase Diagram of PMMCs

Based on the observed behavior of short and long cracks in PMMCs, six crack growth regimes were identified by Li and Ellyin [11]: unstable growth, long crack growth; near-threshold long crack growth; short crack growth; pre-cease short crack growth, and non-growth phases. Figure 8 combines all of the above six phases in a diagram which displays the range of applied stress amplitude and crack length for each phase. Each phase boundary corresponds or is related to an overall material property.

The short crack growth (**SG**)

Short crack growth takes place at high stress amplitudes bounded on the ordinate by the fatigue limit σ_{fl} and the fracture stress σ_f, corresponding to a crack length of an average particle diameter, d. (There is often a cracked particle in the composite due to manufacturing process.)

As the crack grows, the required applied stress to drive it decreases. The short crack grow rate, as discussed earlier, is dominated by the local stress, as depicted by the da/dN vs. a, diagram at the top-left corner of Fig. 8. These cracks generally grow along the slip bands, however, in the PMMCs, both the size and shape of the crack-tip plastic zone is affected by the nearby particle.
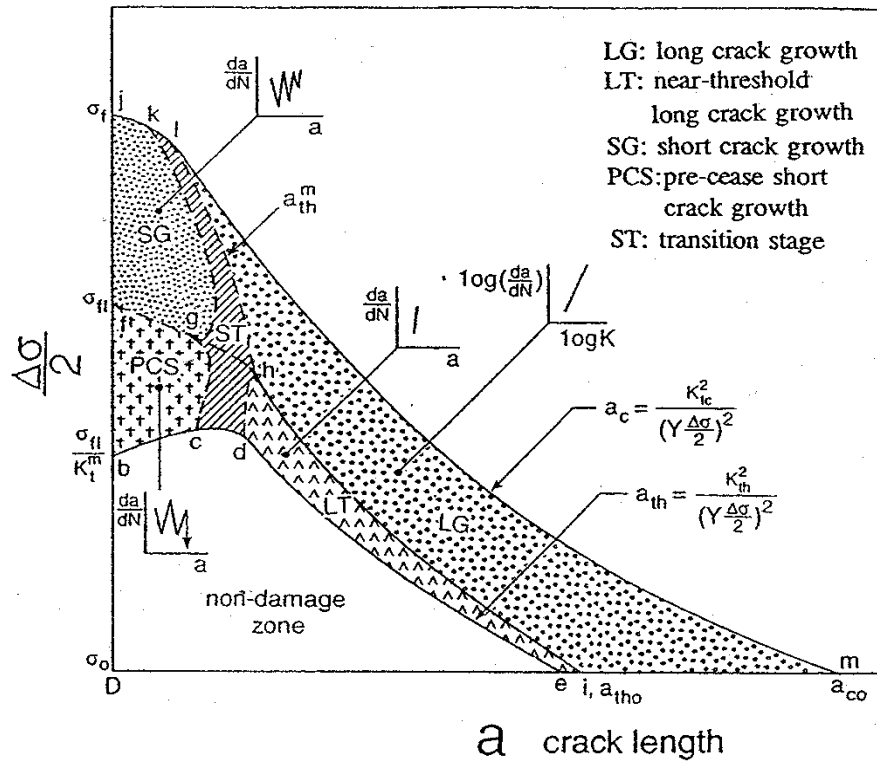
Figure 8. Crack phase diagram of particle-reinforced metal matrix composites, from [11].

The pre-cease short crack phase **(PCS)**

This regime is bound between the fatigue limit stress, σ_{fl}, and an applied stress of σ_{fl} / K_t^m where K_t^m is a local material stress concentration factor

$$K_t^m = \Delta\sigma_{loc} / \Delta\sigma_{appl} \tag{10}$$

where $\Delta\sigma_{loc}$ is a local stress range averaged over a representative volume. With the increased crack length the influence of local stress decreases, and σ_{fl} / K_t^m represents a local stress equal to the fatigue limit of the bulk material.

Near-threshold long crack growth **(LT)**

This phase is depicted in Fig. 8, by a growth characteristic which corresponds to lower stresses than those of short cracks but a longer crack length, and a very steep growth rate. The cracks in this zone generally propagate along a slip band in the matrix. The particles along the crack path generally tend to debond rather than crack. The lower boundary of this phase corresponds to the threshold condition,

$$a_{th} = \frac{\Delta K_{th}^2}{(Y\Delta\sigma/2)^2}, \quad \frac{\Delta\sigma}{2} < \sigma_{fl} \tag{11}$$

where *Y* is a crack geometric factor.

The long crack growth (**LG**)

This phase is bound at its upper boundary by the critical condition of unstable crack growth. This condition is governed by the material toughness, i.e. the critical stress intensity value determined from the resistance curve,

$$a_c = \frac{\Delta K_c^2}{(Y\Delta\sigma/2)^2} \tag{12}$$

For higher values of stress, ΔK_c, is to be substituted by an elastic-plastic parameter. At the long growth regime and intermediate ΔK, the plastic zone is of a multiple slip nature. The resistance of a particle to the crack advance depends on the cyclic plastic zone ahead of a nearby crack. At the threshold for the long crack growth, ΔK_{th}, the plastic zone (slip band) length is not long enough to extend over the neighboring particle and to crack it.

In summary, each of the above crack growth phase boundaries corresponds to a certain material property. In the case of short cracks, they are strength parameters in terms of stress, i.e. σ_f or σ_{fl} whereas for the long cracks they are related to the stress intensity factors, e.g. ΔK_c or ΔK_{th}. The short crack regime in PMMCs is more extensive than that of the matrix alloy, and the plastic zone shape varies as the crack tip approach a particle, as depicted in Fig. 8. Further discussion on the crack tip cyclic plasticity patterns can be found in Ellyin and Li [15].

CONCLUSIONS

- Short cracks up to 400 microns in length grow under the fatigue limit of the metal matrix composite in a shear dominated mode with drastically varied growth rate and with bowing and branching mechanisms due to the local particle dependency.

- With an increase in the applied stress range and/or increased length, the microstructure sensitivity of short crack growth decreases. This appears to be a consequence of the transition from a single slip band at the crack tip to a multiple slip-plastic zone.

- A common characteristic of the particulate reinforced metal matrix composites is that the long crack growth rate in the intermediate range of ΔK, is independent of the reinforced particle. This is in contrast to the near threshold ΔK_{th} values where there is a strong influence of the particles.

- A crack phase diagram for particle reinforced metal matrix composites was presented. It indicated the range of the applied stress and crack length for different crack growth mechanisms in these materials.

- A series of finite element models were constructed to study the effect of particle size, particle spacing (volume fraction), particle fracture and debonding on the crack tip stress, strain and opening displacement (CTOD) of a nearby short crack. The analysis provided an understanding of the mechanism of short crack trapping/untrapping in the particle reinforced metal matrix composites.

REFERENCES

1. Lloyd, D.J. (1994). In: *Intrinsic and Extrinsic Fracture Mechanisms in Inorganic Composite Systems*, pp. 39-47, Lewandowski, J.J. and Hunt, Jr., W.H. (Eds.) TMS Publ.
2. Davidson, D.L.(1991). M*etall. Trans. A*, **18A**, 2115-2138.
3. Ellyin, F., Xia, Z., Li, C.-S.(2005). In: *Fracture and Damage of Composites*, pp. 73-103, Guagliano, M. and Aliabadi, M.H. (Eds.), WIT Press, USA.
4. Christman, T., Suresh, S. (1988). *Acta Metall. Mater.* **36**, 1691-1704.

5. Poza, P. (1996). Doctoral Thesis, Polytechnic University of Madrid, Spain.

6. Xia, Z., Ellyin, F. and Meijer, G. (1997). *Compos. Sci. Technol.* **57**, 237-248.

7. Meijer, G., Xia, Z. and Ellyin, F. (1997). A*cta Metall. Mater*. **45,** 3237-3249.

8. Ellyin, F. (1997). *Fatigue Damage, Crack growth and Life Prediction,* Chapman & Hall, London.

9. Li, C.-S., Ellyin, F. (1995). *Metall. Trans*. **26A**, 3177-3182.

10. Li, C.-S., Ellyin, F. (1994). *Compos. Sci. Technol.* **52**, 117-124.

11. Li, C.-S., Ellyin, F. (1995). *Fatigue Fract. Engng. Mater. Struct*. **18**, 1299-1309.

12. Shang, J.K., Ritchie, R.O. (1998). *Acta Metall*. **37**, 2267-2278.

13. Ellyin, F. (1986). *Engng. Fract. Mech*. **25**, 463-473.

14. Fine, M.E., Davidson, D.L. (1983). In: ASTM STP, **811**, pp. 350-368, Philadelphia, PA.

15. Ellyin, F., Li, C.-S. (1995). *Mater. Sci. Research Int*. **1**, 137-143.